Available online at www.sciencedirect.com
ScienceDirect
Trans. Nonferrous Met. Soc. China 28(2018) 235−243
Transactions of Nonferrous Metals Society of China
www.tnmsc.cn

Microstructures and mechanical properties of semi-solid squeeze casting ZL104 connecting rod

Yong-fei WANG, Sheng-dun ZHAO, Chen-yang ZHANG

School of Mechanical Engineering, Xi'an Jiaotong University, Xi'an 710049, China

Received 12 September 2016; accepted 21 April 2017

Abstract: Semi-solid squeeze casting (SSSC) and liquid squeeze casting (LSC) processes were used to fabricate a ZL104 connecting rod, and the influences of the process parameters on the microstructures and mechanical properties were investigated. Results showed that the tensile strength and elongation of the SSSC-fabricated rod were improved by 22% and 17%, respectively, compared with those of the LSC-fabricated rod. For SSSC, the average particle size (APS) and the shape factor (SF) increased with the increase of re-melting temperature (T_r), whereas the tensile strength and elongation increased first and then decreased. The APS increased with increasing the mold temperature (T_m), whereas the SF increased initially and then decreased, which caused the tensile strength and elongation to increase initially and then decrease. The APS decreased and the SF increased as squeezing pressure (p_s) increased, and the mechanical properties were enhanced. Moreover, the optimal T_r, p_s and T_m are 848 K, 100 MPa and 523 K, respectively.
Key words: aluminum alloy; semi-solid squeeze casting; semi-solid microstructure; tensile strength; elongation; connecting rod

1 Introduction

A semi-solid metal forming (SSMF) process combines the advantages of a traditional hot forging and casting because of the thixotropic characteristics of a semi-solid slurry [1−4]. Furthermore, squeeze casting (SC) can achieve near-net shape metal parts in only one forming step with superior mechanical properties because of the high-pressure solidification behavior of SC [5,6]. Semi-solid squeeze casting (SSSC) is a combination of SSMF and SC; the semi-solid slurry can flow steadily, which decreases the porosity that often occurs in liquid squeeze casting (LSC) [7,8]. Meanwhile, the semi-solid slurry will be solidified under high pressure, which can also further enhance the mechanical properties of the castings [5]. Additionally, the formed parts can also undergo heat treatment to further improve their mechanical properties. Therefore, SSSC can increase material utilization, simplify production process and improve product quality [9].

The microstructures and mechanical properties in SSSC are different from those in liquid forming processes [10−12]. BURAPA et al [13] studied the effects of primary phase morphology on the mechanical properties of Al−Si−Mg−Fe alloy during the SSSC process and concluded that the ultimate tensile strength and elongation increased as the primary α(Al) particle size decreased and the shape factor (SF) increased. LEE and KANG [14] investigated the injection velocity and solid volume fraction of the semi-solid slurry during the vertical rheological SC of a front-wheel suspension support, and fine microstructure and mechanical properties were obtained when the solid fraction was 0.5 and the injection velocity was 1.0 m/s. DAI et al [15] studied the effects of optimal parameters, including squeezing pressure (p_s), mold temperature (T_m) and heat treatment, on the microstructure and mechanical properties of rheological SC of Al−Cu−5Mn−Ti alloy. They found that the tensile strength and elongation were improved by 6.5% and 47%, respectively, compared with the conventional SC samples. Therefore, the microstructure and mechanical properties of the SSSC were affected not only by p_s, but also by re-melting temperature (T_r), and T_m. However, few studies have reported the effect of the process parameters on fabricating a ZL104 connecting rod by SSSC.

ZL104 alloy is a widely used hypoeutectic

Foundation item: Project (51335009) supported by the National Natural Science Foundation of China; Project (2014JQ7273) supported by the Natural Science Foundation of Shaanxi Province of China; Project (CXY1514 (1)) supported by the Xi'an Science and Technology Plan Projects, China
Corresponding author: Yong-fei WANG; Tel: +86-13488126840; E-mail: yongfeio@126.com
DOI: 10.1016/S1003-6326(18)64656-4

Al−Si−Mg based aluminum alloy, which is advantageous for SSSC because of its relatively wide solidification range and superior semi-solid formability. Therefore, the present study aims to compare the microstructure and mechanical properties in the fabrication of a connecting rod with SSSC and LSC and in optimizing the main process parameters to obtain the best microstructure and mechanical properties.

2 Experimental

2.1 Material

The commercial ZL104 aluminum alloy was used as an experimental material, and its chemical compositions are presented in Table 1. Differential scanning calorimetry (DSC) analysis was conducted to obtain the semi-solid range. From the result, the solidus and liquidus temperatures for the ZL104 alloy were 828 and 871 K, respectively.

Table 1 Chemical compositions of commercial ZL104 alloy (mass fraction, %)

Si	Mn	Mg	Zn	Fe	Cu	Al
9.32	0.3	0.24	0.2	0.2	0.05	Bal.

2.2 Procedure

Figure 1 illustrates a common aluminum connecting rod casting, which is widely used in the automobile industry. The casting consists of two same connecting rods linked by two branch runners and a main runner.

Before the experiments, a semi-solid aluminum alloy billet prepared by electromagnetic stirring (EMS) was machined to remove the oxide skin and surface defects. The semi-solid bar (*d*60 mm × 100 mm) was partially re-melted in a resistance furnace at 838−853 K for 20 min. Meanwhile, the mold was preheated to the preset temperature, and then the lubricant was sprayed uniformly. Finally, the re-melted billet was placed in the barrel of the SC machine, and SSSC was performed at the preset parameters. The p_s was applied to the billet from the gate of the mold cavity, and it was held until solidification was completed. The LSC was also conducted for comparison. The specific experimental parameters are displayed in Table 2. The T6 heat treatment of the connecting rod was conducted as follows: the rods were isothermally held at 808 K for 3 h, quenched in water at 343 K, and then isothermally held at 448 K for 10 h.

Table 2 Different experimental parameters for LSC and SSSC

Parameter	Variable	Invariant
T_r/K	843, 848, 853, 923	T_m=523 K, p_s =100 MPa
p_s/MPa	50, 75, 100	T_r=848 K, T_m=523 K
T_m/K	473, 523, 573, 623	T_r=848 K, p_s =100 MPa

2.3 Microstructure and mechanical properties

The metallographic specimen was cut from an arm of connecting rod A. All samples were ground, polished, and etched with an aqueous solution of 0.5% HF. The microstructural observation was conducted using an

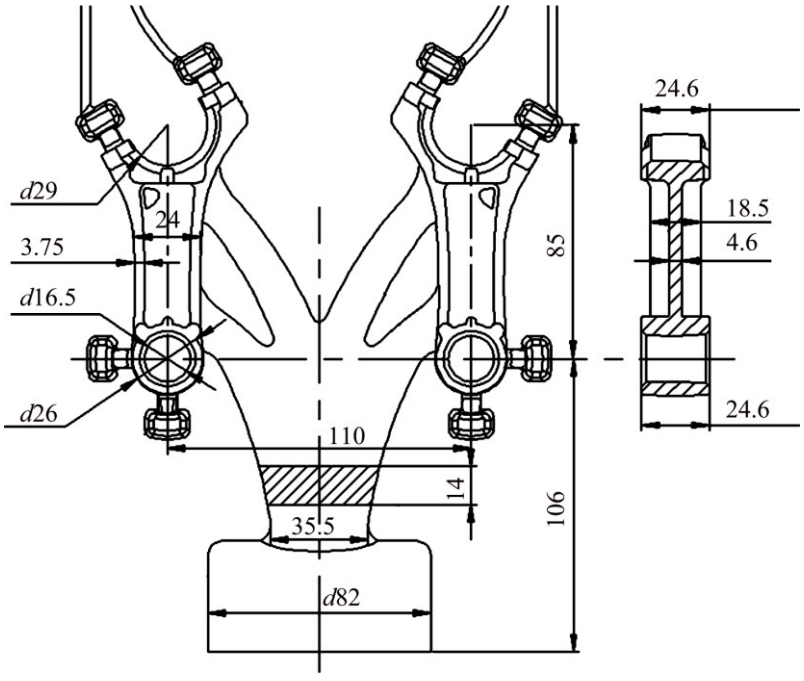

Fig. 1 Schematic diagram of connecting rod casting (unit: mm)

Olympus GX5 optical microscope. The average particle size (APS) and SF were calculated by using Eqs. (1) and (2) [16,17]. The tensile specimen (ASTM E8) was obtained from connecting rod B and tested on a universal material testing machine at a tensile rate of 1.25 mm/min.

$$\mathrm{APS}=\frac{\sum_{N=1}^{N}\sqrt{4A/\pi}}{N} \tag{1}$$

$$\mathrm{SF}=\frac{\sum_{N=1}^{N}4\pi A/P^2}{N} \tag{2}$$

where P is the perimeter of the particle; A is the area of the particle; and SF is a value varying from zero (for acicular particles) to one (for a perfectly round sphere).

3 Results and discussion

3.1 Microstructure of raw material and semi-solid slurry prepared by EMS and typical connecting rods fabricated by SSSC

Figure 2 shows the microstructure of a raw material. As shown in Fig. 2, the ZL104 alloy has a typical dendritic microstructure, and the coarse primary and secondary dendrites have obvious orientations. Moreover, the primary and secondary dendrite arm spaces were approximately 100 and 20 μm, respectively.

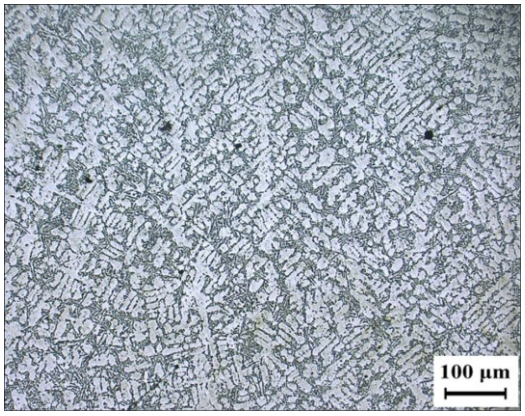

Fig. 2 Microstructure of commercial ZL104 alloy

Compared with Fig. 2, the microstructure of the EMS-treated ZL104 semi-solid billet was fine, and the evenly distributed non-dendritic structure is illustrated in Fig. 3(a). The near-spherical particles were separated by numerous lathy needle-shaped eutectic silicon owing to the relatively high silicon content in the ZL104. The partial re-melted microstructures of the EMS-treated semi-solid billet presented isolated and spherical particles that were evenly distributed in the eutectic phase (Fig. 3(b)) when the re-melting temperature was 853 K and the isothermal holding time was 20 min. The APS and SF were 32 μm and 0.76, respectively. Liquid pockets were trapped in some large spherical grains because the adjacent non-dendritic particles were merged with one another during the partial re-melting process. The needle-shaped eutectic silicon evolved into a thick strip or a broken lump around the spherical grains.

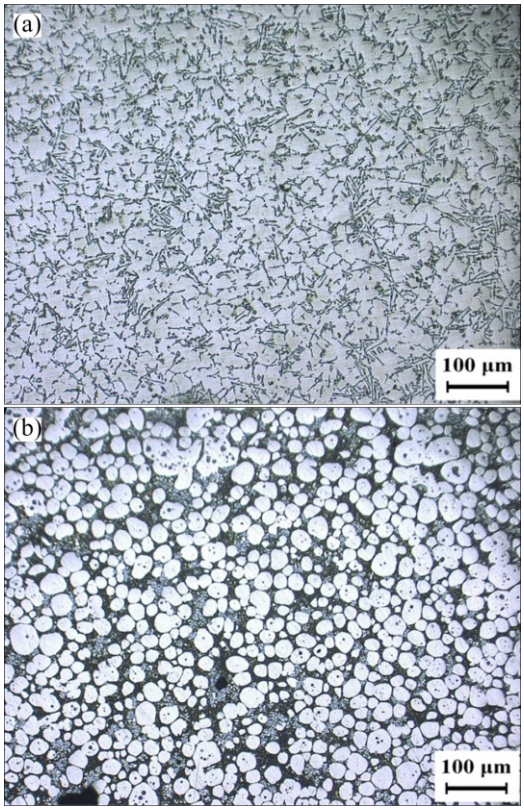

Fig. 3 Microstructures of ZL104 semi-solid slurry: (a) After EMS treatment; (b) After partial re-melting

The mold cavity under different parameters can be filled fully, and the typical connecting rod fabricated by SSSC (T_r=848 K, p_s=100 MPa, and T_m=523 K) is presented in Fig. 4. The casting was filled perfectly with sharp outlines and fine surface because of the close contact between the slurry and the mold cavity, which demonstrates the good flow ability and formability of the semi-solid slurry.

3.2 Microstructure and mechanical properties of connecting rods fabricated under different re-melting temperatures

Figure 5 illustrates the corresponding microstructure under the T_r of 843, 848, 853, and 923 K (total liquid), p_s of 100 MPa, and T_m of 523 K. In Fig. 5, the microstructure of the connecting rod fabricated by SSSC at different T_r (843−853 K) were mainly composed of large α_1(Al) spherical grains and small α_2(Al) particles that were uniformly distributed in the eutectic phase. The

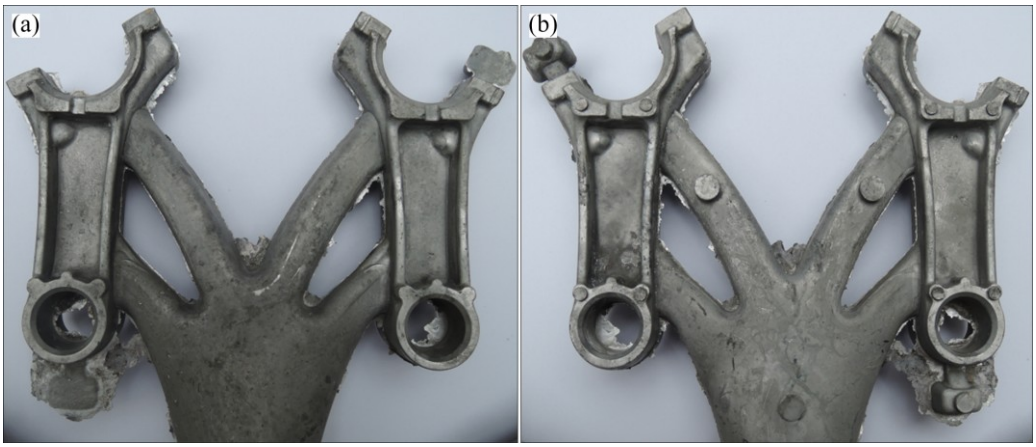

Fig. 4 Typical connecting rod fabricated by SSSC (T_r=848 K, p_s=100 MPa, T_m=523 K): (a) Front; (b) Back

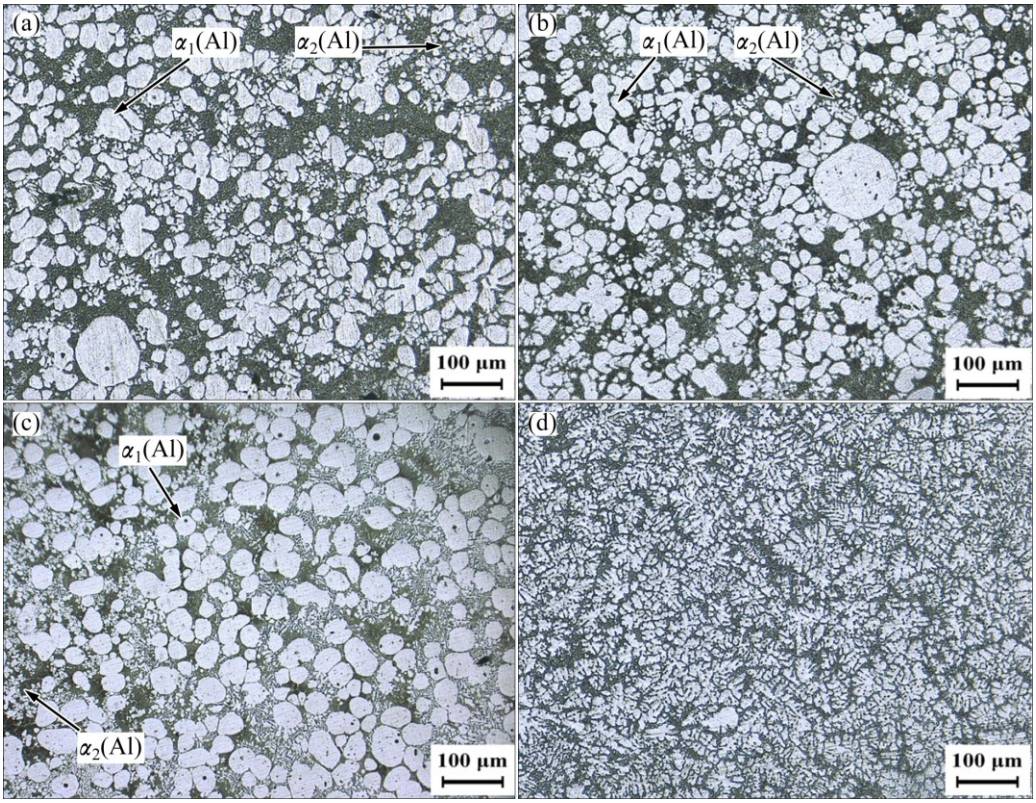

Fig. 5 Microstructures of connecting rod fabricated at different re-melting temperatures: (a) 843 K; (b) 848 K; (c) 853 K; (d) 923 K (total liquid)

APS of α_1(Al) spherical grains was 30−50 μm, whereas that of the α_2(Al) particles was about 10 μm. However, the microstructure of the LSC-fabricated connecting rod (923 K) mainly consisted of fine dendrites and eutectic phases distributed among the dendrite arms as depicted in Fig. 5(d).

The formation of the microstructures during the SSSC process can be divided into two stages [18]. First, the primary α(Al) reserved in the partial remelting process was further coarsened during the mold filling and the high-pressure solidification processes, which finally grew into large and spherical α_1(Al) grains. Second, heterogeneous nucleation occurred in the residual liquid phase, and the crystal nucleus further grew into fine α_2(Al) particles under high applied pressure during the filling and pressure-retaining processes [18]. The α_2(Al) particles could not grow fully during the rapid solidification process because of the low T_m and the thin wall of the connecting rod casting. Therefore, most α_2(Al) particles showed poor morphology.

Figure 6 depicts that the APS and SF increased with

the increase of T_r. The microstructure presented fine spherical α_1(Al) grains and numerous small α_2(Al) particles with irregular shapes when the T_r was 843 K, resulting in small APS and SF values of α_1(Al) and α_2(Al) particles. When the T_r increased to 848 K, the α_1(Al) grains did not grow coarser, whereas the α_2(Al) particles became coarser, and the spheroidization degree was further improved. Therefore, the APS and SF slowly increased. The coarse α_1(Al) grains became more spherical with a further increase of T_r up to 853 K, whereas the α_2(Al) particles were too small for calculation, leading to a rapid increase of APS and SF.

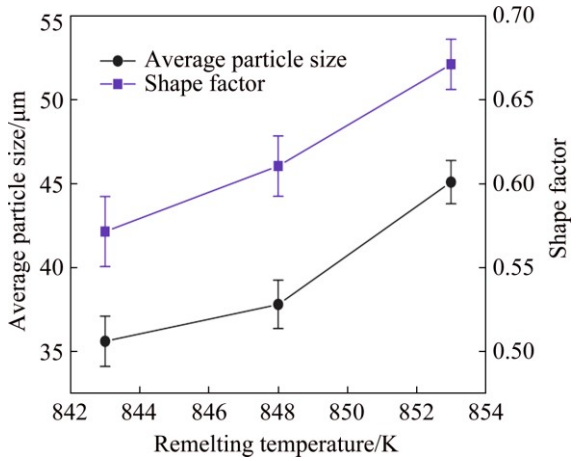

Fig. 6 Variations of APS and SF with different re-melting temperatures

Figure 7 presents the histogram of tensile strength and elongation with different T_r for the connecting rod fabricated by SSSC and LSC. The tensile strength and elongation increased first and then decreased as T_r increased, and the maximum values were obtained at 848 K. Furthermore, the tensile strength and elongation of the SSSC-fabricated rod were obviously improved by 22% and 17%, respectively, compared with those of the LSC-fabricated rod, which may be due to the typical dendritic structure in the LSC-fabricated rod.

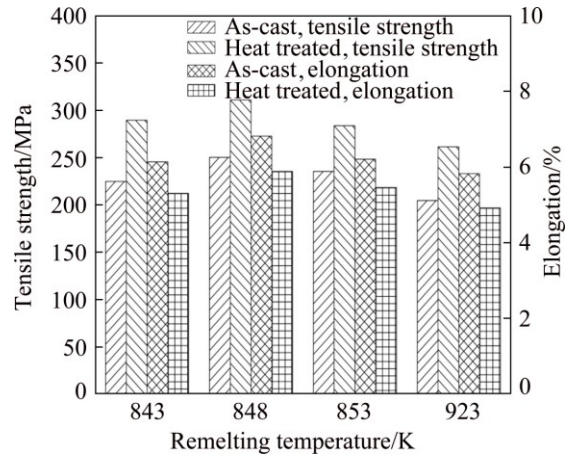

Fig. 7 Tensile strength and elongation variations with different re-melting temperatures

A similar trend in the mechanical properties was reported with the increase of pouring temperature in the LSC, which was attributed to the low pouring temperature refined the microstructure but deteriorated the cast densification, causing the mechanical properties to first increase and then decrease [9]. Similarly, low pouring temperature also refined the microstructure in SSSC; however, the decreased mechanical properties may be mainly caused by the morphology and size of the α(Al) grains, especially the α_2(Al) particles. At low T_r, a high undercooling rate led to the sharp increase of nucleation rate. Finally, the crystal nucleus developed into a number of fine α_2(Al) particles with irregular shapes, as illustrated in Fig. 5(a). The spheroidization degree of the α_1(Al) grains was further improved with the increase of T_r, whereas the α_2(Al) particles further grew into more spherical ones evenly distributed around the α_1(Al) grains (Fig. 5(b)). The homogeneous distribution and good morphology of the α_2(Al) particles improved the tensile strength and elongation at 848 K compared with those at 843 K. However, the sufficient liquid phase at high T_r (853 K) ensured that the α_1(Al) grains completely grew into coarse spherical grains, whereas small α_2(Al) particles were developed from a limited number of crystal nucleus during the filling process under applied pressure (Fig. 5(c)), which may deteriorate mechanical properties. Therefore, 848 K was the optimal T_r in the SSSC process.

Figure 7 also demonstrates that the T6 heat treatment increased the tensile strength of both SSSC-fabricated and LSC-fabricated rods and decreased their elongation. By comparison, the tensile strength and elongation of SSSC remained higher than those of LSC by 19% and 20%, respectively. The flaky eutectic silicon was transformed into a granular eutectic silicon, and other fine intermetallic compound precipitates were dispersed from the supersaturated solid solution, which surrounded the grain boundary of the α(Al) particles during the T6 heat treatment. The refinement and morphological change of the eutectic phase remarkably affected the mechanical properties [15]. These precipitates inhibited the dislocation and enhanced the tensile strength of the alloy. However, some precipitated phases may damage the continuity of the aluminum alloy matrix, and the stress concentration at these points could accelerate the formation and extension of cracks, which may reduce the toughness and elongation of the alloy.

3.3 Microstructure and mechanical properties of connecting rod fabricated under different squeeze pressures

Figure 8 shows the microstructure of the connecting rod under the p_s of 50, 75, and 100 MPa, T_r of 848 K, and T_m of 523 K. The corresponding variations of the APS

and SF with increasing p_s are illustrated in Fig. 9. Some coarse rosette-like α_1(Al) grains and non-uniformly distributed α_2(Al) particles with irregular shapes were found under the p_s of 50 MPa (Fig. 8(a)). The α_1(Al) grains transformed into spherical and fine ones with further increase in p_s. Particularly at 100 MPa, the spheroidization degree of the α_1(Al) grains was further improved, and small α_2(Al) particles were distributed around them as presented in Fig. 9(c). A few large rosette-like α_1(Al) grains transformed into more spherical ones as p_s increased from 50 to 100 MPa. This transformation may be due to the coalescence of the neighboring grains with similar orientations during the filling and pressure solidification processes. In Fig. 9, the increased p_s reduced APS and improved SF. In addition, the downtrend of APS and the uptrend of SF were gradually decreased when p_s exceeded 75 MPa.

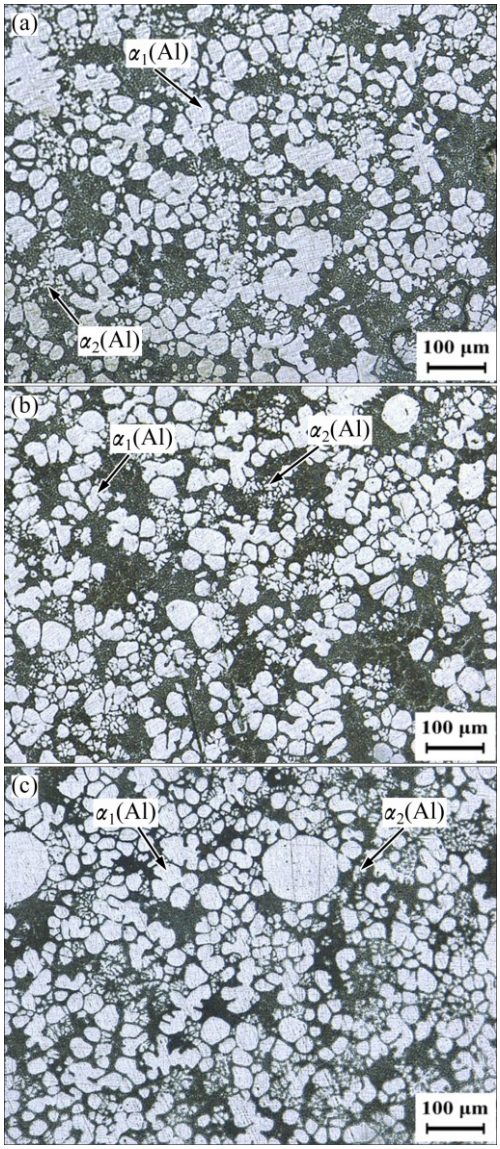

Fig. 8 Microstructures of connecting rod fabricated by SSSC under different squeezing pressures: (a) 50 MPa; (b) 75 MPa; (c) 100 MPa

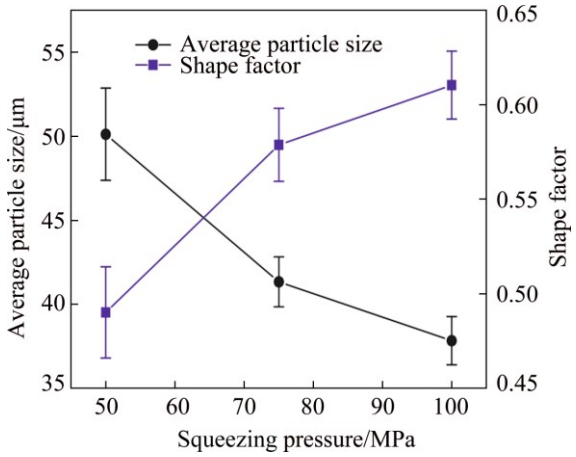

Fig. 9 Variations of APS and SF with different squeezing pressures

The influence of p_s on the microstructural evolution during the SSSC could be attributed to the increased solidification temperature and cooling rate of the slurry [8]. First, Clausius−Clapeyron equation can be used to indicate the effect of p_s on the solidification temperature [15,19].

$$\frac{\Delta T_f}{\Delta p}=\frac{\Delta T_f(V_l-V_s)}{\Delta H_f} \tag{3}$$

where T_f is the equilibrium solidification temperature; V_l and V_s are the specific volumes of the liquid and solid, respectively; ΔH_f is the latent heat of fusion, and p is the applied pressure. Equation (3) indicates that solidification temperature increases with pressure, which leads to a high degree of undercooling, resulting in grain refinement and spheroidization. Moreover, a high p_s promotes the close contact between the semi-solid slurry and the mold. Consequently, the heat transfer coefficient and cooling rate were increased [20], inhibiting the excessive coarsening of the α_1(Al) and α_2(Al) grains. Hence, APS was decreased, and SF was increased with the increase of p_s, as depicted in Fig. 9.

Figure 10 illustrates the tensile strength and elongation variations with p_s. The tensile strength and elongation of the castings increased with the increase of the p_s, with or without T6 heat treatment. The tensile strength and elongation were increased obviously when p_s increased from 50 to 75 MPa. However, growth slowed down to a stable state at 100 MPa. Based on investigating the LM13 alloy SC [21], when p_s exceeded 100 MPa, the mechanical properties would not improve obviously. First, the casting densification may be maximized because the semi-solid slurry and the mold surface achieved a completely close contact [21]. Only a slight improvement in the microstructure was attained because the effect of the p_s reached some dynamic balance with the grain refinement. Moreover, excessively

high applied pressure may damage the mold and equipment. Therefore, the p_s for SSSC should be limited to 100 MPa.

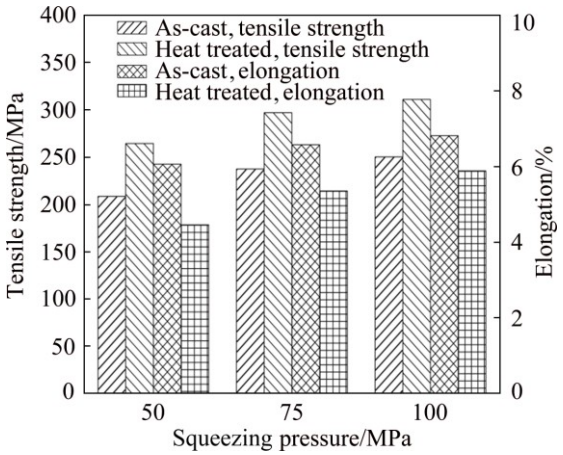

Fig. 10 Tensile strength and elongation variations with different squeezing pressures

3.4 Microstructures and mechanical properties of connecting rod fabricated at different mold temperatures

Figure 11 depicts the corresponding microstructures at the T_m of 473, 523, 573, and 623 K, T_r of 848 K, and p_s of 100 MPa. When T_m was 473 K, some rosette-like α_1(Al) grains and small and irregularly shaped α_2(Al) particles formed (Fig. 11(a)). The α_1(Al) grains were coarsened, and the morphology was improved as T_m increased to 523 K, whereas the α_2(Al) particles grew slightly, as shown in Fig. 11 (b). With further increase in T_m, the α_1(Al) grains further grew into large and spherical grains, and the α_2(Al) particles gradually changed to small dendritic particles located around the α_1(Al) grains as illustrated in Figs. 11(c) and (d).

Figure 12 shows the effect of T_m on APS and SF. The APS was increased with the increase of T_m, whereas SF was increased at first and then decreased when the T_m exceeded 573 K. This phenomenon was caused by the numerous dendritic α_2(Al) particles that coalesced with the α_1(Al) grains at 573 and 623 K. Figure 13 shows tensile strength and elongation variations with T_m. The mechanical properties of the castings at 523 K were obviously higher than those at 473 K. However, further increase in T_m from 523 to 623 K could decrease the tensile strength and elongation.

At low T_m, high undercooling degree caused the rapid solidification of the slurry, which markedly increased the amount of α_2(Al) particles. However, α_1(Al) grains and α_2(Al) particles cannot grow and coarsen because of the high heat transfer coefficient and cooling rate. Consequently, the morphologies of α_1(Al) grains and α_2(Al) particles deteriorated, resulting in small APS and SF. Moreover, the solidified skin may form on the surface of the mold cavity because of the chilling effect. The skin was broken into pieces and drawn into the casting during the high pressure filling [15]. All these factors resulted in the poor

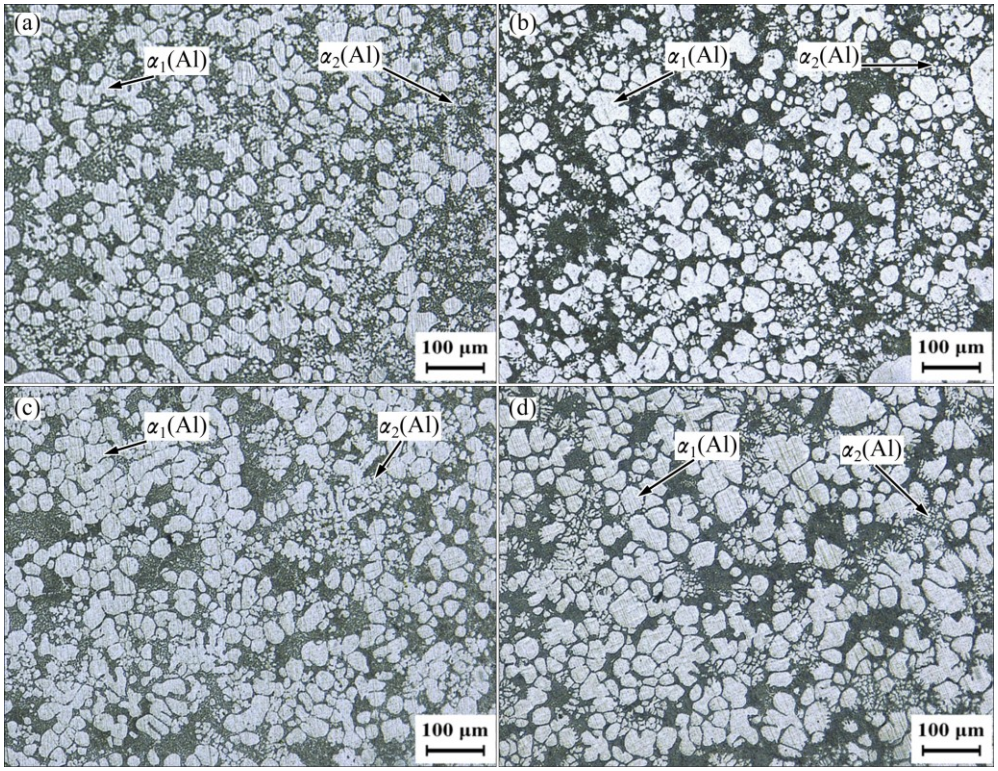

Fig. 11 Microstructures of connecting rod fabricated by SSSC at different mold temperatures: (a) 473 K; (b) 523 K; (c) 573 K; (d) 623 K

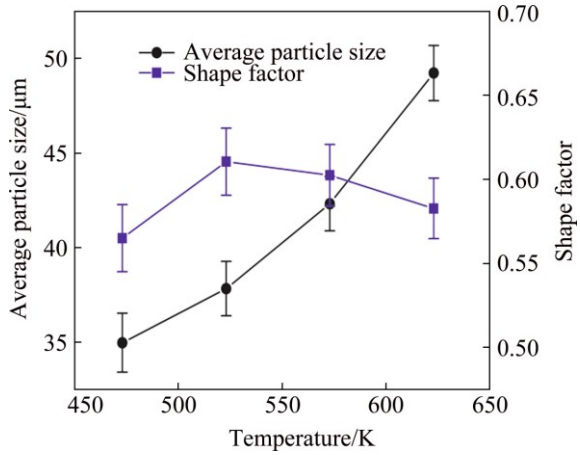

Fig. 12 APS and SF variations with mold temperature

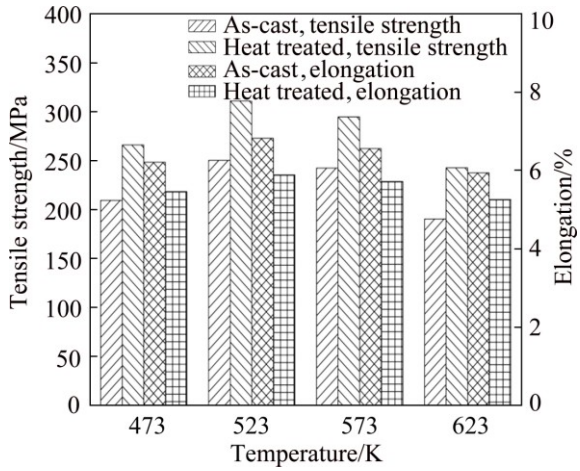

Fig. 13 Tensile strength and elongation variations with mold temperatures

mechanical properties at low T_m. On the contrary, at high T_m, the α_1(Al) grains grew excessively, and some of them coalesced with one another, forming irregularly shaped grains, whereas the α_2(Al) particles grew into small dendrites and attached to the coarse α_1(Al) grains. The deteriorative morphology of the α(Al) grains reduced the tensile strength and elongation of the castings. Based on the results, the T_m for SSSC should be restricted to approximately 523 K.

According to the experimental results presented in this study within a certain range of the parameters, the optimal microstructure and mechanical properties of the connecting rod fabricated by SSSC were obtained. The optimal parameters were T_r=848 K, p_s=100 MPa, and T_m=523 K. Under these parameters, the tensile strength and elongation of SSSC were obviously improved by 22% and 17%, respectively, than those of LSC before the T6 heat treatment; they were also increased by 19% and 20%, respectively, than those of LSC after the T6 heat treatment.

4 Conclusions

1) Compared with the LSC-fabricated connecting rod, the tensile strength and elongation of SSSC-fabricated connecting rod improved by 22% and 17%, respectively. These increases were mainly attributed to the improved morphology, as well as the size of the fine α_1(Al) grains and the small α_2(Al) particles in SSSC.

2) Both APS and SF increased with the increase of T_r, whereas tensile strength and elongation increased first and then decreased. The best mechanical properties were obtained at 848 K.

3) The APS decreased with the increase of p_s, whereas the SF increased. The tensile strength and elongation were enhanced as p_s increased.

4) Both APS and SF increased with the increase of T_m, thereby enhancing the mechanical properties. However, when the T_m exceeded 573 K, the APS further increased, whereas the SF decreased, and the mechanical properties of the connecting rod were deteriorated.

5) The optimal process parameters in the SSSC for the fabrication of the connecting rod are as follows: T_r is 848 K, p_s is 100 MPa, and T_m is 523 K.

References

[1] GUAN Ren-guo, ZHAO Zhan-yong, ZHANG Qiu-Sheng, LEE C S, LIU Chun-ming. Effect of the casting temperature on temperature field and microstructure of A2017 alloy during an innovative continuous semisolid rolling process with a vibrating sloping plate device [J]. International Journal of Advanced Manufacturing Technology, 2013, 67(1−4): 917−923.

[2] JIANG Ju-fu., WANG Ying, LIU Jun, QU Jian-jun, DU Zhi-ming, LUO Shou-jing. Microstructure and mechanical properties of AZ61 magnesium alloy parts achieved by thixo-extruding semisolid billets prepared by new SIMA [J]. Transactions of Nonferrous Metals Society of China, 2013, 23(3): 576−585.

[3] HU Zhao-Hua, WU Guo-Hua, ZHANG Peng, LIU Wen-Cai, PANG Song, ZHANG Liang, DING Wen-Jiang. Primary phase evolution of rheo-processed ADC12 aluminum alloy [J]. Transactions of Nonferrous Metals Society of China, 2016, 26(1): 19−27

[4] SALLEH M S, OMAR M Z, ALHAWARI K S, MOHAMMED M N, MAMALI M A, MOHAMAD E. Microstructural evolution and mechanical properties of thixoformed A319 alloys containing variable amounts of magnesium [J]. Transactions of Nonferrous Metals Society of China, 2016, 26(8): 2029−2042

[5] HUANG X S, HE L J, MI G B, LI P J. Characteristics of defect bands and their formation mechanisms in A356 wheel fabricated by horizontal squeeze casting [J]. Materials Science and Technology, 2014, 31(4): 400−408.

[6] LU Shu-lin, WU Shu-sen, NIU Z, AN P, MAO Y. Effect of semi-solid processing on microstructure and mechanical properties of 5052 aluminum alloy [J]. Transactions of Nonferrous Metals Society of China, 2015, 20(S3): s758−s762.

[7] CHEN Qiang, YUAN Bin, ZHAO Gao-zhan, SHU Da-yu, HU Chun-kai, ZHAO Zu-de, ZHAO Zhi-xiang. Microstructural evolution during reheating and tensile mechanical properties of thixoforged AZ91D-RE magnesium alloy prepared by squeeze casting–solid

extrusion [J]. Materials Science and Engineering A, 2012, 537(2): 25−38.
[8] ASHIRI R, KARIMZADEH F, NIROUMAND B. On effect of squeezing pressure on microstructural characteristics, heat treatment response and electrical conductivity of an Al−Si−Mg−Ni−Cu alloy [J]. Materials Science and Technology, 2014, 30(10): 1162−1169.
[9] DAO V, ZHAO Sheng-dun, LIN Wen-jie, ZHANG Chen-yang. Effect of process parameters on microstructure and mechanical properties in AlSi9Mg connecting rod fabricated by semi-solid squeeze casting [J]. Materials Science and Engineering A, 2012, 558(51): 95−102.
[10] MO Wen-fei, ZHAND Liang, WU Guo-hua, ZHANG Yang, LIU Wen-cai WANG Cun-long. Effects of processing parameters on microstructure and mechanical properties of squeeze-cast Mg−12Zn−4Al−0.5Ca alloy [J]. Materials and Design, 2014, 63: 729−737.
[11] LIN Bo, ZHANG Wei-wen, LUO Zhao-Hui, ZHANG Da-tong, LI Yuan-yuan. Comparative study on microstructures and mechanical properties of the heat-treated Al−5.0Cu−0.6Mn−*x*Fe alloys prepared by gravity die casting and squeeze casting [J]. Materials and Design, 2014, 59: 161−168.
[12] MASOUMI M, HENRY H. Influence of applied pressure on microstructure and tensile properties of squeeze cast magnesium Mg−Al−Ca alloy [J]. Materials Science and Engineering A, 2011, 528 (10−11): 3589−3593.
[13] BURAPA R, JANUDOM S, CHUCHEEP R, CANYOOK J, WANNASIN J. Effects of primary phase morphology on mechanical properties of Al−Si−Mg−Fe alloy in semi-solid slurry casting process [J]. Transactions of Nonferrous Metals Society of China, 2010, 20(S3): s857−s861.
[14] LEE S M, KANG C G. Effect of solid fraction on formability and mechanical properties in a vertical-type rheo squeeze-casting process [J]. Proceedings of the Institution of Mechanical Engineers (Part B): Journal of Engineering Manufacture, 2011, 225(B2): 184−196.
[15] DAI Wei, WU Shu-sen, LU Shu-lin, LIN Chong. Effects of rheo-squeeze casting parameters on microstructure and mechanical properties of AlCuMnTi alloy [J]. Materials Science and Engineering A, 2012, 538: 320−326.
[16] XU Yan, HU Lian-xi, JIA Jian-bo, XU Bo. Microstructure evolution of a SIMA processed AZ91D magnesium alloy based on repetitive upsetting-extrusion (RUE) process [J]. Materials Characterization, 2016, 118: 309−323.
[17] TAO Jiang-quan, JIANG Ju-fu, CHEN Hong, XIAO Yuan-lun, ZHANG Rong-chao, HUA Hu-qiang, ZHAO Jun, ZHAO Qiang. Application of cyclic upsetting-extrusion to semi-solid processing of AZ91D magnesium alloy [J]. Transactions of Nonferrous Metals Society of China, 2013, 23(4): 909−915.
[18] HITCHCOCK M, WANG Yun, FAN Z. Secondary solidification behaviour of the Al−Si−Mg alloy prepared by the rheo-diecasting process [J]. Acta Materialia, 2007, 55(5): 1589−1598.
[19] WU Shu-sen, ZHONG Gu, AN Ping, WAN Li. ZHONG J X X. Microstructural characteristics of Al−20Si−2Cu−0.4Mg−1Ni alloy formed by rheo-squeeze casting after ultrasonic vibration treatment [J]. Transactions of Nonferrous Metals Society of China, 2012, 22(12): 2863−2870.
[20] VIJIAN P, ARUNACHALAM V P. Optimization of squeeze cast parameters of LM6 aluminium alloy for surface roughness using Taguchi method [J]. Journal of Materials Processing Technology, 2006, 180(3): 161−166.
[21] MALEKI A, NIROUMAND B, SHAFYEI A. Effects of squeeze casting parameters on the microstructure of LM13 alloy [J]. Journal of Materials Processing Technology 2009, 209(8): 3790−3797.

半固态挤压铸造铝 ZL104 合金连杆的显微组织及力学性能

王永飞，赵升吨，张晨阳

西安交通大学 机械工程学院，西安 710049

摘　要：分别采用液态挤压铸造和半固态挤压铸造工艺成形 ZL104 铝合金连杆，研究不同工艺参数对连杆的显微组织及力学性能的影响规律。结果表明：与传统液态挤压铸造相比，半固态挤压铸造连杆的抗拉强度和伸长率分别提高了 22%和 17%。半固态挤压铸造过程中，随着重熔温度的增加，平均晶粒尺寸和形状因子都增大；随着模具预热温度的升高，平均晶粒尺寸增大，形状因子先增加后减小；这两种情况下连杆的抗拉强度和伸长率都先增加后减小。但随着挤压压力的提高，平均晶粒尺寸减小，且形状因子增大，连杆的力学性能明显提高。此外，成形半固态挤压铸造连杆的最佳重熔温度、挤压压力及模具预热温度分别为 848 K、100 MPa 及 523 K。

关键词：铝合金；半固态挤压铸造；半固态显微组织；抗拉强度；伸长率；连杆

(Edited by Xiang-qun LI)